ELSEVIER

Journal of Structural Geology 29 (2007) 411–421

JOURNAL OF STRUCTURAL GEOLOGY

www.elsevier.com/locate/jsg

The Rigid Grain Net (RGN): An alternative method for estimating mean kinematic vorticity number (W_m)

Micah J. Jessup [a,*], Richard D. Law [a], Chiara Frassi [b]

[a] *Department of Geosciences, Virginia Tech., Derring Hall, Blacksburg, VA 24061, USA*
[b] *Dipartimento di Scienze della Terra, Università di Pisa, 56126 Pisa, Italy*

Received 7 June 2006; received in revised form 1 November 2006; accepted 17 November 2006
Available online 22 January 2007

Abstract

The use of porphyroclasts rotating in a flowing matrix to estimate mean kinematic vorticity number (W_m) is important for quantifying the relative contributions of pure and simple shear in penetratively deformed rocks. The most common methods, broadly grouped into those that use tailed and tailless porphyroclasts, have been applied to many different tectonic settings; however, attempts have not been made to unify the various methods. Here, we propose the Rigid Grain Net (RGN) as an alternative graphical method for estimating W_m. The RGN contains hyperbolas that are the mathematical equivalents to the hyperbolic net used for the porphyroclast hyperbolic distribution (PHD) method. We use the RGN to unify the most commonly used W_m plots by comparing the distribution of theoretical and natural tailless porphyroclasts within a flowing matrix. Test samples from the South Tibetan detachment, Tibet yield indistinguishable results when the RGN is compared with existing methods. Because of its ease of use, ability for comparing natural data sets to theoretical curves, potential to standardize future investigations and ability to limit ambiguity in estimating W_m, the RGN makes an important new contribution that advances the current methods for quantifying flow in shear zones.

Keywords: Vorticity; PHD; South Tibetan detachment; Porphyroclast; Mylonite; Shear zone; Gondasampa; Rongbuk Valley

1. Introduction

Attempts to use the aspect ratio and orientation of rigid objects rotating in a flowing matrix to characterize the relative contributions of pure and simple shear (vorticity) began with the pioneering works of Jeffery (1922) and Ghosh and Ramberg (1976). Subsequent investigations contributed to these founding principles by applying the early theory to geologic samples (Passchier, 1987; Simpson and De Paor, 1993, 1997; Wallis, 1992, 1995; Wallis et al., 1993). Rigid porphyroclast analyses are now commonly employed to characterize flow within shear zones in a variety of tectonic settings (e.g., Klepeis et al., 1999; Xypolias and Doutsos, 2000; Holcombe and Little, 2001; Xypolias and Koukouvelas, 2001; Bailey and Eyster, 2003; Law et al., 2004; Jessup et al., 2006; Xypolias and Kokkalas, 2006).

Models for the rotation of elliptical objects in a fluid demonstrate that during simple shear (mean kinematic vorticity number $W_m = 1$) rigid objects will rotate infinitely, regardless of their aspect ratio (R). With increasing contributions of pure shear ($0 < W_m < 1$), porphyroclasts will either rotate with the simple shear component (forward) or against it (backward) until they reach a stable-sink orientation that is unique to R and W_m (Fig. 1; Ghosh and Ramberg, 1976; Passchier, 1987; Simpson and De Paor, 1993, 1997).

Three main analytical techniques (Passchier, 1987; Simpson and De Paor, 1993, 1997; Wallis, 1995) use rigid porphyroclasts to estimate W_m in high strain zones, all of which rely on the same fundamental mathematical relationships between W_m, R or

* Corresponding author. Tel.: +1 540 525 0635; fax: +1 540 231 3386.
E-mail address: mjessup@vt.edu (M.J. Jessup).

0191-8141/$ - see front matter © 2006 Elsevier Ltd. All rights reserved.
doi:10.1016/j.jsg.2006.11.003

Nomenclature

W_m	mean kinematic vorticity number
R	porphyroclast aspect ratio (long axis/short axis)
B^*	shape factor of Bretherton (1962) [Eq. (2)]
M_n	short axis of the porphyroclast
M_x	long axis of the porphyroclast
θ	angle between long axis and the foliation Eq. (1)
$X'_2 - X'_3$	plane normal to the rotational axis
X'_1	rotation axis
β	angle between the stable-sink and source–sink in the $X'_2 - X'_3$ plane [Eq. (3)]
R_c	critical threshold between grains that rotate infinitely and those that reach a stable-sink position.
$R_{c_{min}}$	minimum R_c as defined by Law et al. (2004)
$R_{c_{max}}$	maximum R_c as defined by Law et al. (2004)

shape factor (B^*), and angle of porphyroclast long axis with respect to the macroscopic foliation (θ), to define a critical threshold (R_c) below which they continuously rotate, and above which they record a stable-sink orientation (Table 1; Fig. 2; Jeffery, 1922; Ghosh and Ramberg, 1976). We refer to the Passchier (1987) and Wallis (1995) methods as the Passchier and Wallis plots, respectively (Fig. 3A and B). For the third approach, we use the name porphyroclast hyperbolic distribution (PHD) plot of Simpson and De Paor (1993, 1997) (Fig. 3D).

Because these methods rely on the same founding principles of Jeffery (1922) and Bretherton (1962), they should yield similar W_m estimates. However, prior to this investigation, no attempts were made to compare or unify the three techniques.

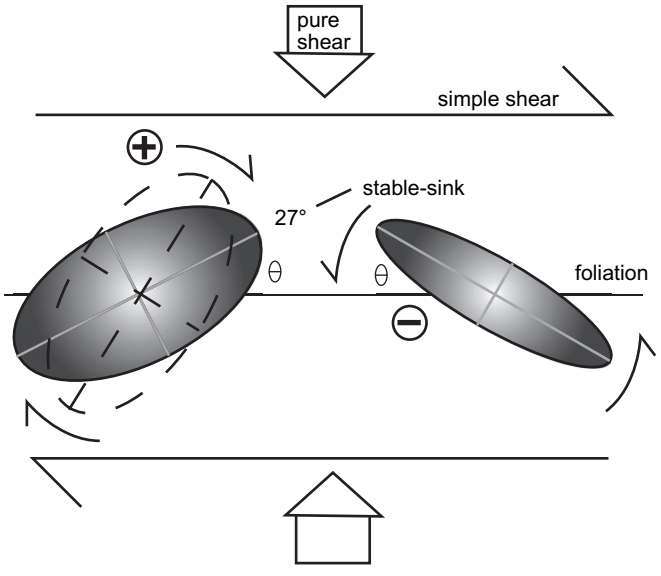

Fig. 1. Rotation of two simplified elliptical porphyroclasts within a regime of general shear. Porphyroclast on the left has an aspect ratio of 2 ($B^* = 0.6$) and is in the stable-sink orientation of $\theta = 27°$ and represents one of many possible original orientations that rotated forward to the stable-sink position. The porphyroclast on the right is back rotated, due to the pure shear component, and has a long axis at a negative angle (θ) to the foliation.

Table 1
Critical threshold values

R	W_m	θ at R_c	B^*	β	cos(β)
1.1	0.1	42	0.1	84	0.1
1.21	0.2	39	0.2	78	0.2
1.3	0.3	36	0.3	73	0.3
1.5	0.4	33	0.4	66	0.4
1.7	0.5	30	0.5	60	0.5
2	0.6	27	0.6	53	0.6
2.4	0.7	23	0.7	46	0.7
3	0.8	18	0.8	37	0.8
4.4	0.9	13	0.9	26	0.9

R = aspect ratio (long axis/short axis).
W_m = mean kinematic vorticity number.
θ = angle from foliation.
R_c = critical threshold.
B^* = shape factor.
β = opening angle of hyperbola.

Without a standard method for estimating W_m by comparing natural data sets to the orientations of porphyroclasts as predicted by Ghosh and Ramberg (1976), ambiguity was introduced into various adaptations of the three methods. To help standardize vorticity analysis using rigid porphyroclast in a flowing matrix, ease plotting of data, and limit ambiguity in estimating W_m, we build on the Passchier plot to create the Rigid Grain Net (RGN); a series of modified semi-hyperbolas that represent the stable configuration of porphyroclasts predicted for specific W_m values. Since the relative importance of sigma- and delta-type tails on these porphyroclast has already received considerable attention (Passchier, 1987; Simpson and De Paor, 1993, 1997), and to make this comparison of techniques applicable to the most common types of porphyroclasts found in mylonitic rocks, we simplify our investigation by treating all data as tailless porphyroclasts. Plots of theoretical and natural tailless porphyroclasts on the RGN, Passchier, Wallis and PHD plots unify the four methods for using rigid tailless porphyroclasts to estimate W_m. By providing a net representing the theoretical orientations of rigid porphyroclasts in a flowing matrix that can be imported into an Excel© chart, against which natural data set can be compared, the RGN offers a less ambiguous, easier to use, alternative method for estimating W_m in high strain zones.

2. Review of techniques

During general shear, rigid grain analysis assumes that the orientation of porphyroclasts within a flowing matrix record a critical threshold (R_c) between porphyroclasts that rotate indefinitely (low aspect ratio), and therefore do not develop a preferred orientation, and those that reach a stable-sink orientation (higher aspect ratio; Fig. 1). This unique combination of W_m, R or B^* and θ define the value of R_c between these two groups of rigid grains (Table 1; Figs. 2 and 3). If a porphyroclast is axially-symmetric, then there is only one stable-sink position. Alternatively, if the porphyroclast is axially non-symmetric, then two stable-sink positions exist (Passchier,

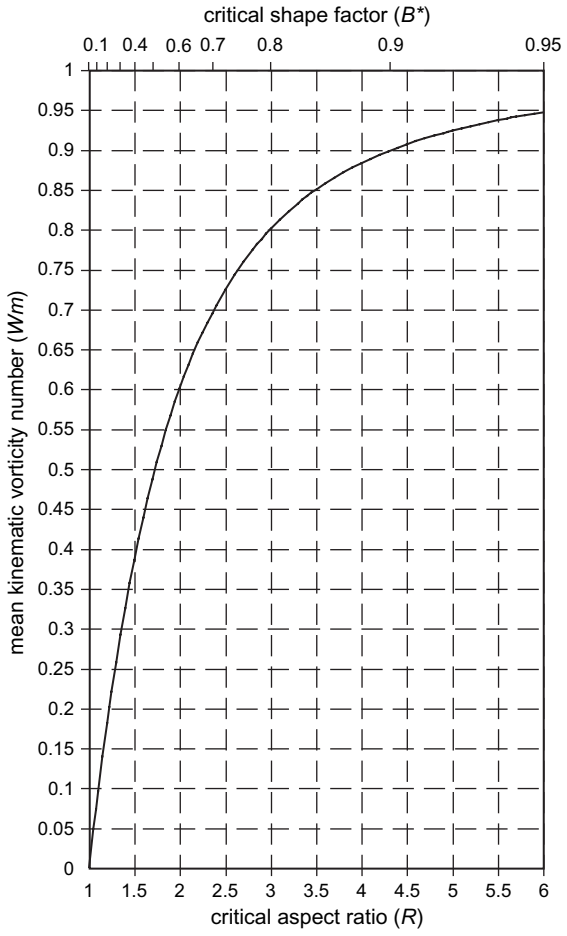

Fig. 2. Plot showing the relationship between mean kinematic vorticity number (W_m), shape factor (B^*), and aspect ratio (R) at critical values.

1987). Passchier (1987) related W_m to B^* and θ through the following equations:

$$\theta = 1/2\sin^{-1}W_m/B^*\left\{\left(1-W_m^2\right)^{1/2}-\left(B^{*^2}-W_m^2\right)^{1/2}\right\} \quad (1)$$

$$B^* = \left(M_x^2-M_n^2\right)/\left(M_x^2+M_n^2\right) \quad (2)$$

where M_n, short axis of clast; M_x, long axis of clast.

Eq. (1) links B^*, W_m and θ and will generate a hyperbolic curve in θ vs. B^* space that represents the ideal distribution of grains for a particular W_m. The vertices of this hyperbola mark the unique R_c value where $W_m = B^*$. Assuming relatively high strain, a natural distribution of porphyroclasts should define a limb of this hyperbola for a range of B^* values that is greater than B^* at R_c. With relatively low strains, a misleading distribution of porphyroclasts has the potential to overestimate the simple shear component because high aspect ratio porphyroclasts have yet to rotate into their stable-sink orientation (Passchier, 1987; Vissers, 1989; Bailey et al., in press). Porphyroclasts with a $B^* < B^*$ at R_c will rotate infinitely and should define a broad distribution with $\theta \pm 90°$. In contrast, porphyroclasts with a $B^* > B^*$ at R_c are predicted to reach stable-sink orientations with a limited range in θ values (Fig. 3A). Whether a porphyroclast will rotate forward or backward to a stable-sink position depends on the initial θ (i.e., prior to the onset of deformation) at a specific B^* and W_m. When treating all porphyroclasts as tailless, R_c should be defined by the distribution of both the orientation and either B^* or R, as well as an abrupt change in range of θ values (Fig. 3A and B).

Passchier (1987) proposed the following equation for the two possible stable-sink orientations for axially non-symmetric objects in the $X_2' - X_3'$ plane:

$$\cos\beta = W_m/B^* \quad (3)$$

where β, angle between the source and sink in the $X_2' - X_3'$ plane; $X_2' - X_3'$, plane normal to the rotational axis (X_1').

The long axis of the porphyroclast is predicted to rotate towards the two stable-sink positions when:

$$W_m < B^* \quad (4)$$

For example, assuming a W_m of 0.6 where $B^* = W_m$, then using Eq. (3), $\beta = 53.13°$, the stable-sink position for a porphyroclast with $R = 2$ has a $\theta = 26.56°$ (Table 1; Fig. 2). Passchier (1987) predicts that when $W_m < B^*$ (i.e., the aspect ratio of the porphyroclasts is greater than when $W_m = B^*$ at R_c), two stable-sink positions for axially non-symmetric objects exist. The positive/negative angles from the foliation for tailless porphyroclasts long axes cannot uniquely define their rotational history (i.e., forward vs. back-rotated sigma and delta porphyroclasts of Passchier, 1987; Simpson and De Paor, 1993).

Although the distribution of porphyroclasts on the original Passchier plots can be informative, particularly for the highest quality data sets (Fig. 3A), without a reference frame for comparing complex natural data with the theoretical values established by Eq. (1), defining R_c will remain ambiguous. Passchier (1987) attributes the deviation of natural samples from orientations predicted by theory to (1) variation of non-axially symmetric porphyroclasts between the two possible stable-sink positions, (2) changes in B^* of porphyroclasts (i.e., shape change) during progressive deformation attributed to recrystallization without instant reorientation of the object, and (3) variation in the frame of reference (e.g., recrystallized tails or foliation).

Wallis (1995) used equations from Passchier (1987) to create the Wallis plot that uses tailless porphyroclasts to define R_c and therefore W_m. The Wallis plot still uses θ on the Y-axis, but replaces B^* with the more intuitive porphyroclast aspect ratio (R = long axis/short axis) on the X-axis (Fig. 3B; Wallis, 1992, 1995). W_m is calculated from the R_c values separating porphyroclasts that reach a stable-sink orientation ($\theta < \theta$ at R_c) from those that rotate continuously ($\theta > \theta$ at R_c). Although using R is more intuitive, W_m estimates cannot be determined directly from the plots, as with the Passchier plot, and must be calculated using the following equation (Wallis et al., 1993):

$$W_m = \left(R_c^2-1\right)/\left(R_c^2+1\right) \quad (5)$$

where R_c, critical aspect ratio.

The distribution of porphyroclasts in natural systems often defines a gradual transition between these two populations

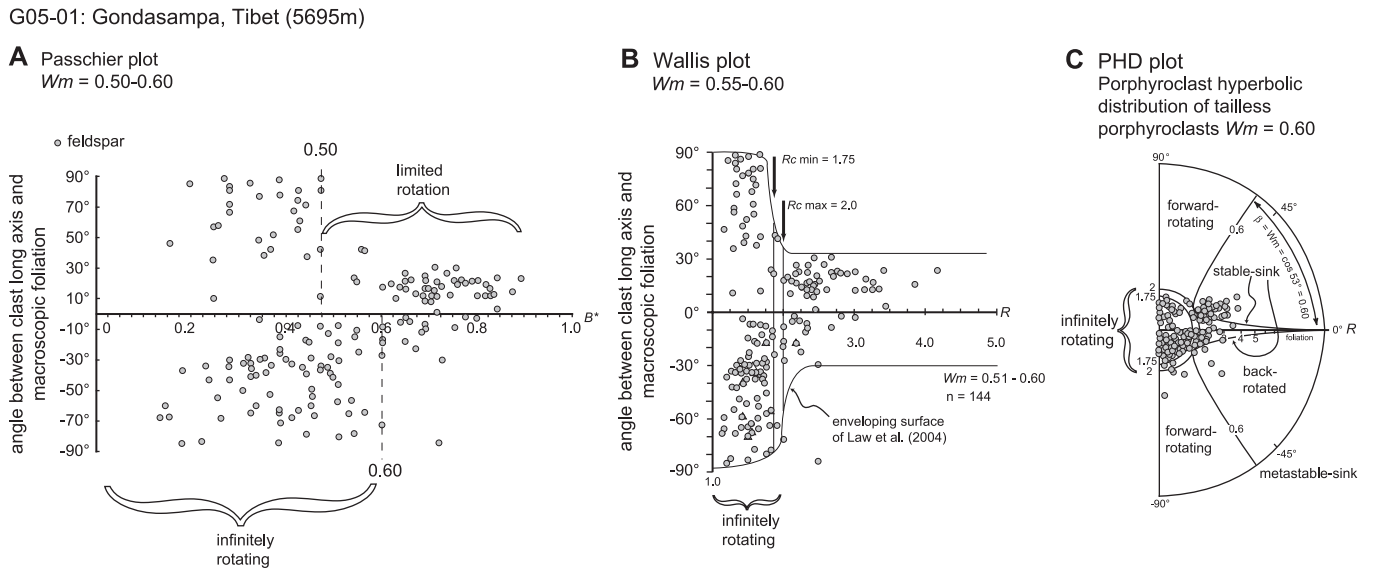

Fig. 3. Examples of tailless porphyroclast data from sample G05-01 plotted using the Passchier plot (A), Wallis plot (B), and the porphyroclast hyperbolic distribution (PHD) plot (C) to estimate mean kinematic vorticity (W_m). The Passchier plot uses the shape factor $B^* = (M_x^2 - M_n^2)/(M_x^2 + M_n^2)$ (where M_n = short axis and M_x = long axis of the porphyroclast) vs. angle between porphyroclast long axis and foliation (θ) to define the critical threshold used to estimate W_m (0.50–0.60). The Wallis plot uses the aspect ratio (R = long axis/short axis) and angle from macroscopic foliation (θ) to locate the critical threshold (R_c). W_m is calculated using R_c where $W_m = (R_c^2 - 1)/(R_c^2 + 1)$. Upper and lower R_c values are used to estimate a range in likely W_m estimates of 0.51–0.60. The PHD plot uses the hyperbolic net to plot aspect ratio (R) and θ. Following the methods of Simpson and De Paor (1993) the cosine of the opening angle (β) of the best-fit enveloping hyperbola yields a W_m estimate of 0.60.

using the Wallis plot, instead of an abrupt change between continuously rotating (random orientation) porphyroclasts and stable- to semi-stable porphyroclasts that define R_c. In response, researchers modified the original Wallis plot by creating an enveloping surface to better-define the grain distribution (Fig. 3B), and use a range in possible W_m values ($R_{c_{min}}$ and $R_{c_{max}}$; Fig. 3B; Law et al., 2004; Jessup et al., 2006). Xypolias and Kokkalas (2006) also plot the best-fit curve using Eq. (1) for a specific W_m as a comparison with their natural data. As with the Passchier plot, ambiguity exists without an external reference frame created by theoretical curves that help justify which porphyroclasts are used to define R_c.

The porphyroclast hyperbolic distribution (PHD) method estimates W_m by using R and the angle between the pole to foliation and long axis of tailed porphyroclasts (Fig. 3C), plotted using the hyperbolic net (HN; De Paor, 1983; Simpson and De Paor, 1993, 1997). Each hyperbola of the HN represents the theoretically predicted orientation of porphyroclasts for a particular R and W_m as plotted in polar coordinates. The opening angle of each hyperbola = β. The vertex of each hyperbola defines R_c, and θ at R_c, for each W_m value. This relationship between stable-sink orientation, as defined by Passchier (1987; Cartesian coordinates) in Eq. (1), and the hyperbolic net (HN; De Paor, 1983; polar coordinates) is established in Eq. (11) of Simpson and De Paor (1993):

$$B^* = W_m/\cos(2\theta) \tag{6}$$

As with Passchier (1987), when $B^* = W_m$ porphyroclasts reach their stable-sink orientation at the minimum angle from the foliation, R_c is defined as the vertices of the hyperbola. One limb of the hyperbola represents the stable-sink orientation for porphyroclasts while the other is the metastable position (i.e., the source–sink position of Passchier, 1987; Fig. 3C). At $\theta >$ the metastable orientation, porphyroclasts will rotate forward until they define another semi-hyperbolic cluster on the concave side of the same hyperbola. Assuming significant shear, back-rotated clasts with variable aspect ratios, plotted on the HN, should define a semi-hyperbolic cluster representing the stable-sink orientation. The linear cluster is then rotated to find the best-fit hyperbola whose limbs represent the two eigenvectors of flow, one of which is asymptotic to the foliation (i.e., the source–sink and stable-sink positions of Passchier, 1987). The vertex of this hyperbola separates the low aspect ratio porphyroclasts with random orientation (i.e., infinitely rotating), from higher aspect ratio porphyroclasts with a narrow range of orientations (Fig. 3C).

3. The Rigid Grain Net (RGN)

Prior to this investigation, the relationship between the PHD, Wallis and Passchier plots was largely unaddressed, particularly using only tailless porphyroclasts. To explore this further, we propose the RGN as an alternative method for estimating W_m. To create the RGN, we modified the Passchier plot and then tested the compatibility of results obtained from the RGN, Wallis and PHD plots using theoretical and natural data sets of tailless porphyroclasts. Eq. (1) was used to calculate semi-hyperbolas for a range of W_m values that express the relationship between θ and B^* (Fig. 4, location A). The second set of curves represent the possible R_c (vertices curves)

values for when $W_m = B^*$ (Fig. 4, location B; Table 1). Each semi-hyperbola was calculated for a particular W_m and a series of B^* values. We use the shape factor (B^*, Eq. (2)) as defined by Bretherton (1962) and subsequently employed by Passchier (1987) because it enables W_m values to be obtained directly from the RGN.

For the RGN, positive and negative semi-hyperbolas are plotted at 0.025 increments for a range in W_m (0.1–1.0) by solving for θ using Eq. (1) ($\theta = \theta$ at R_c, when $B^* = W_m$). For a particular shape factor, when $B^* = W_m$ and $\theta > \theta$ at R_c, the semi-hyperbolas transition into vertical lines to define the maximum B^* value below which grains begin to rotate freely (Fig. 4, location C; Passchier, 1987). To highlight the continuity in R_c values for the range in W_m values represented by the RGN, a second curve (vertices curve) links the R_c values on each hyperbola (Fig. 4, location B). To relate the more intuitive aspect ratio (R) of the Wallis plot to B^* values, they are placed below the B^* values on the X-axis of the RGN (Fig. 4, location D). Together the semi-hyperbolas and R_c curves for positive and negative θ values define the RGN against which natural data sets can be compared (Fig. 4).

To relate hyperbolas on the HN and the RGN, we plot the full hyperbolas on the RGN, highlight the critical curves used to define a $W_m = 0.6$, and plot a hypothetical distribution of porphyroclasts (Fig. 5). The two hyperbolas that are included on the simplified HN are highlighted in black on the RGN ($W_m = 0.6$) for positive and negative θ (Fig. 5A and B). Clasts whose initial orientation plots within any of the stability fields represented by the hyperbolas will, given the slightest perturbation, rotate towards a stable-sink position (Ghosh and Ramberg, 1976). If axially symmetric, these grains will reach a single stable-sink position, whereas axially non-symmetric porphyroclasts (whose $B^* > W_m$) will potentially reach two stable-sink positions (Eqs. (3) and (4)). For porphyroclasts that plot on the metastable limb (locations a–d of Fig. 5A and B) of the negative hyperbola, they will respond to any component of pure shear by back rotating until they reach a stable-sink position, as dictated by their R and W_m, to define a semi-hyperbolic linear cluster (locations e–i, Fig. 5A and B). Porphyroclasts with original orientations outside of the metastable limb of the hyperbola will rotate forward, until they reach the convex side of the stable limb of the hyperbola. Forward rotating grains that accumulate between the two stable limbs of the negative and positive hyperbolas have an $R > R$ at R_c (Eq. (3) and (4)).

Fields of the HN and RGN plots that represent the maximum aspect ratio for porphyroclasts that are predicted to rotate forward infinitely, and thereby have a complete range in θ between $\pm 90^\circ$, are represented by a circle of constant R for all orientations that is tangential to the vertex of each hyperbola and plotted on the center of the HN (i.e., when $B^* < W_m$; Figs. 3C, 5A and C). On the RGN, this area includes all of the potential range in B^* between 0 and B^* at R_c (i.e., to the left of the apex of the hyperbolas; Fig. 5B and D). An additional section of the RGN is highlighted on the HN that defines porphyroclasts that will rotate to the vertices curve for R_c values $\geq$ the "true" R_c for the sample. On the HN, this curve is defined by linking the R_c value from each potential hyperbola greater than the "true" R_c for this sample to generate a small section of the vertices curve as shown on the RGN (Fig. 5A and C). This important clarification shows that these porphyroclasts must be considered as stable-sink orientations

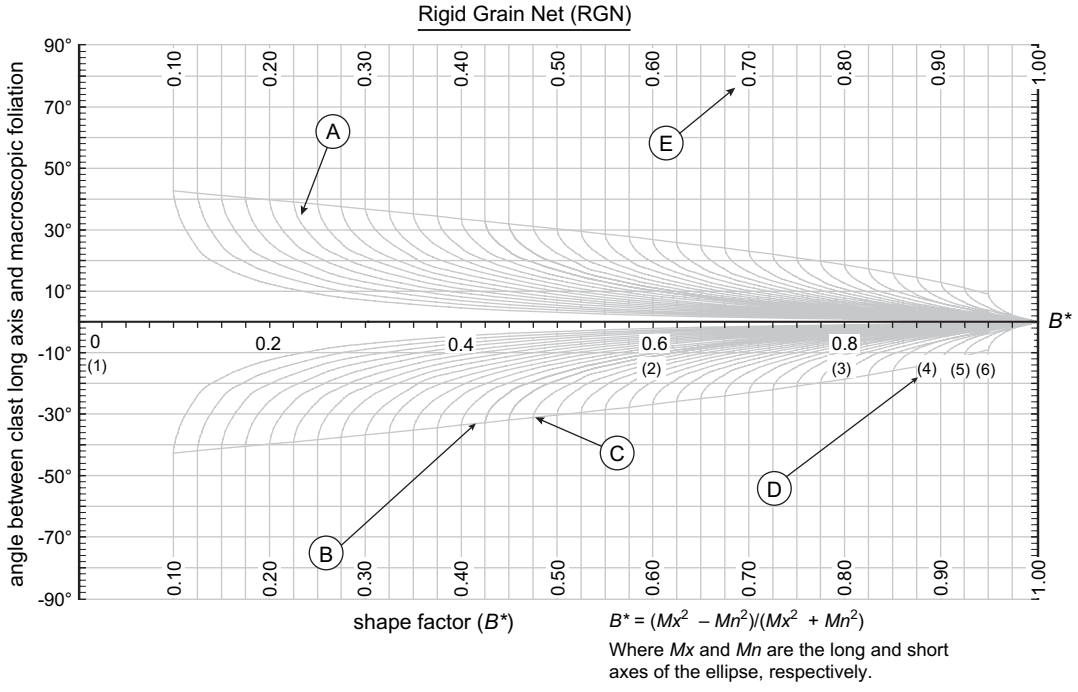

Fig. 4. The Rigid Grain Net (RGN) using semi-hyperbolas. Location A is an example of a semi-hyperbola; location B highlights the vertices curve; location C is an example of a R_c value when $W_m = B^*$; location D points to one of a series of aspect ratio (R) values included on the RGN to demonstrate its relationship with the less intuitive shape factor (B^*); location E is a W_m value for a semi-hyperbola. See text for details.

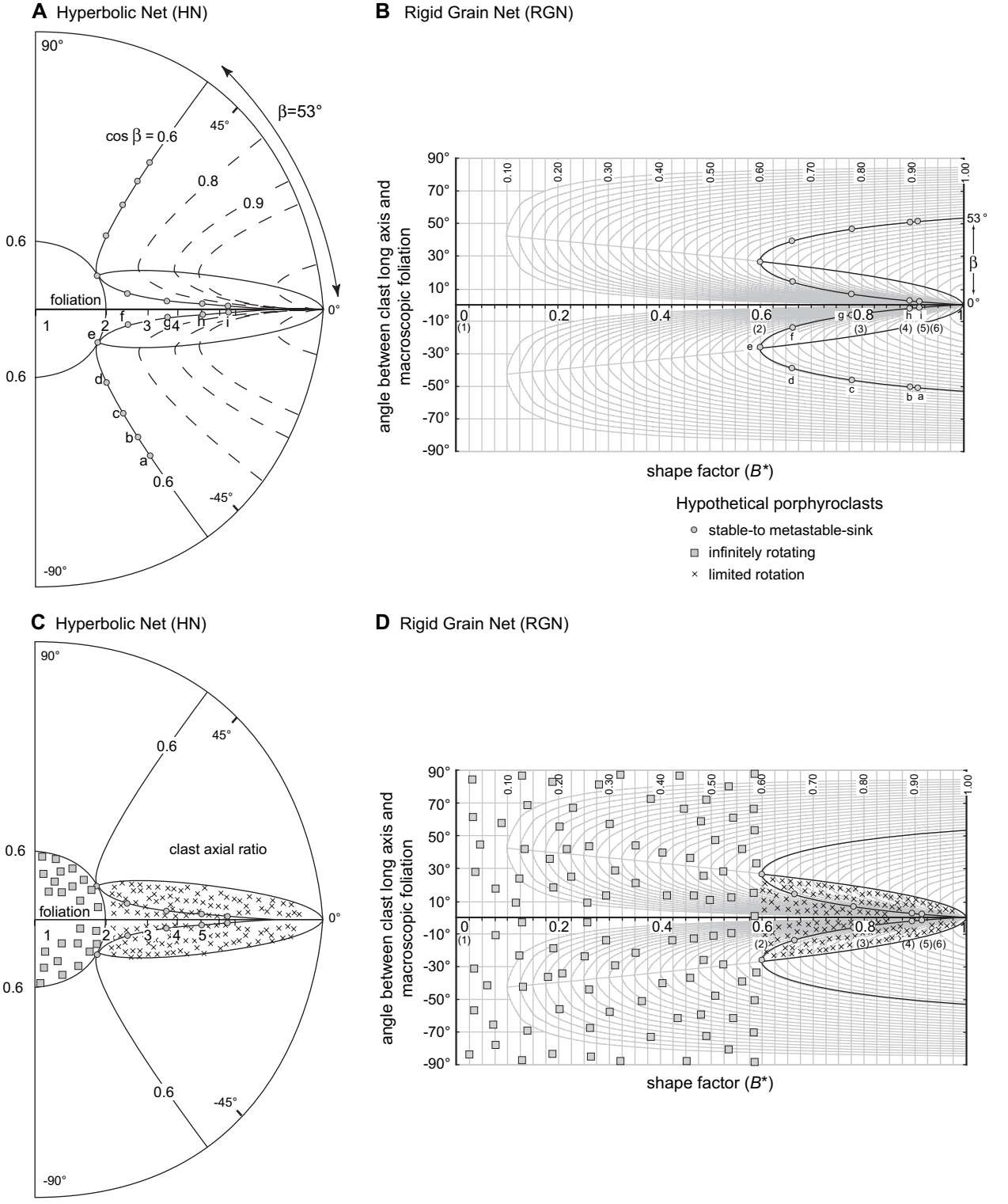

Fig. 5. (A) Half of the hyperbolic net (HN) simplified to graphically demonstrate the relationship between one hyperbola ($W_m = 0.60$) and the vertices curve for that hyperbola. The vertices curve is drawn using the vertices of several hyperbolas (dashed) for a range in W_m values greater than the W_m for the sample (0.60). Gray circles with letters (a–i) on the hyperbola for $W_m = 0.60$ are shown to compare how these define the hyperbolas on the HN and RGN (B). The circle that defines the highest aspect ratio ($R = 2$) below which porphyroclasts are predicted to rotate infinitely is also included. (B) The RGN with complete hyperbolas. Highlighted in black are the positive and negative hyperbolas that correspond to a $W_m = 0.60$, as well as the section of the vertices curve for $B^* > B^*$ at R_c. A series of gray circles represent equivalent points on the RGN and HN. (C) The same plot as (A) with an overlay of different types of hypothetical porphyroclasts in their predicted distribution; gray squares are infinitely rotating, black crosses are limited rotation, gray circles are stable- to metastable-sink positions. (D) The same plot as (B) with hypothetical porphyroclasts distributed in various sections of the RGN.

when choosing the best-fit hyperbola. Because the hyperbolas on the HN and RGN with full hyperbolas are mathematical equivalents, an ideal data set of tailless or tailed porphyroclasts (i.e., $R = 2.0$ and $W_m = 0.60$) are predicted to define this hyperbola on both plots. According to Passchier (1987), all grains with the slightest B^* above B^* at R_c will reach a stable-sink position (crosses of Fig. 5C and D), whereas those below will rotate infinitely and therefore could potentially reach $\theta = \pm 90^\circ$ (gray squares of Fig. 5C and D).

A major benefit to using the RGN is that data can be entered into an Excel© worksheet, as they are obtained on the microscope, and plotted directly on a RGN that is imported as a background to an Excel© chart. This enables the user to immediately monitor how the distribution of porphyroclasts is developing during data acquisition. Each measured porphyroclasts can be compared to the theoretically predicted curves on the RGN. As the plot evolves, the porphyroclasts that define R_c should become obvious. With increased use, the RGN may provide a means to calibrate the results of future investigations (see appendix for a reproducible version of the RGN and the data repository for a JPEG© image of the RGN for use on Excel© charts and an Excel© worksheet).

4. A natural test: the South Tibetan detachment, Tibet

Ultra-mylonitic leucogranite samples from the South Tibetan detachment (STD), exposed near Gondasampa and Rongbuk Valley, Tibet, are particularly well-suited for testing the hypotheses presented above, as well as for demonstrating the utility of the RGN. Samples are from within the upper 30 m of the north-dipping ductile shear zone that marks the transition from the metamorphic core of the Greater Himalayan Slab to overlying unmetamorphosed Cambro-Ordovician limestone. Similar mylonitic leucogranites in the area are dated ~17 Ma by Murphy and Harrison (1999) who suggest that this provides a maximum age for ductile fabric development in Rongbuk Valley. Oriented samples were cut parallel to the stretching lineation and perpendicular to the foliation. When possible, rigid porphyroclasts from multiple thin sections were used. All samples are characterized by feldspar porphyroclasts (lacking evidence for internal plastic deformation) that are widely separated from each other within a foliated matrix of dynamically recrystallized quartz grains (Fig. 6). Elongate tails of recrystallized quartz surround many of the rigid feldspar porphyroclasts. Although many of these porphyroclasts have sigma- and delta-type tails, in order to clarify this comparison between different rigid grain methods for defining W_m, they are treated as tailless. Matrix quartz grains contain bulging grain boundaries and rims of strain-free subgrains that suggest a combination of grain boundary migration and subgrain rotation recystallization accommodated deformation at conditions intermediate between Regimes 2 and 3 of Hirth and Tullis (1992) and temperatures of ~490–530 °C (Stipp et al., 2002). Previous petrofabric investigations in Rongbuk Valley, demonstrated that deformation was characterized by plane strain deformation and supported monoclinic shear (Law et al., 2004; Jessup et al., 2006).

The choice of rigid porphyroclasts was highly selective, ignoring all but the most appropriate grains for estimating W_m (Simpson and De Paor, 1993, 1997). Two samples (G05-01 and G05-03) were selected to test the RGN and how it relates to the PHD and Wallis plots (Fig. 7). PHD plots contain

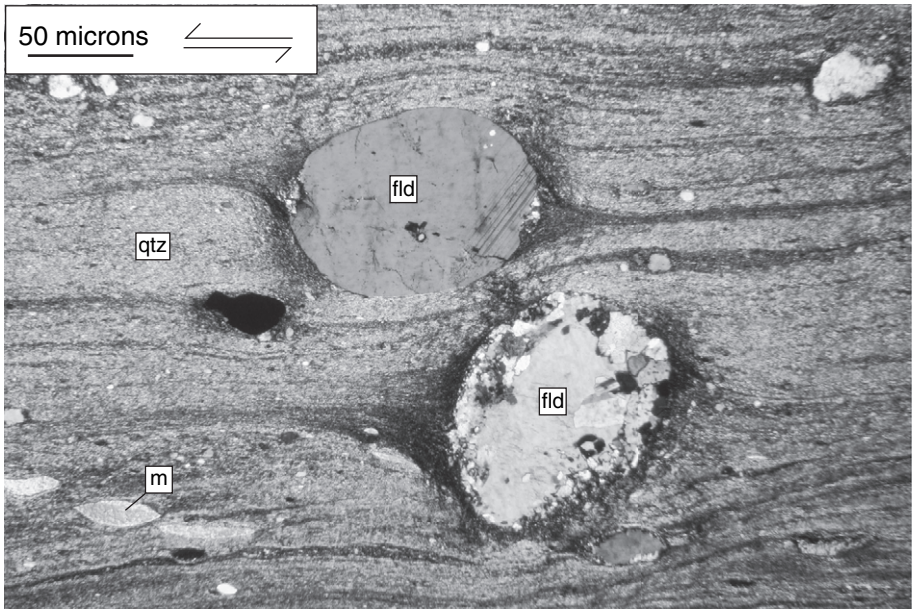

Fig. 6. Photomicrograph with crossed polars of a typical section of sample G05-01 (collected at an altitude of 5695 m). Section cut perpendicular to foliation and parallel to lineation. Abbreviations used for various phases are: m, white mica; fld, feldspar; qtz, quartz. Although representative of the types of porphyroclasts in the thin section, because they are in such close proximity to each other, these two porphyroclasts are unsuited for the RGN.

hyperbolas in the positive and negative fields as well as sections of the vertices curves. Because we are treating all these porphyroclasts as tailless, it is important to clarify that positive and negative θ values cannot uniquely determine whether porphyroclasts followed a forward- or back-rotated path in the sense of Passchier (1987) and Simpson and De Paor (1993, 1997).

Two thin sections of sample G05-01 contain 175 porphyroclasts, with a range in aspect ratios inclined at positive and negative θ values, which are appropriate for rigid grain analysis (Fig. 7A). On the Wallis plot, these grains define an upper and lower R_c of 2.0 and 1.75 ($W_m = 0.60-0.51$), respectively. We interpret the porphyroclast with anomalously high θ and R values as an outlier. Using the PHD method, tailless porphyroclasts were plotted on the HN. To distinguish the R_c value between porphyroclasts that rotated infinitely and those that reached a stable-sink position, excluding the obvious outlier, we choose two circles ($R = 1.75-2.0$) on the HN that envelopes porphyroclast that reach $\pm 90°$. The distribution of porphyroclasts with negative θ values defines a slightly higher R_c ($R = 2$) than for positive ($R_c = 1.75$) values. Positive and negative hyperbolas were then chosen that envelope the majority of the data and touch the R_c value (circle $R = 2.0$) of the infinitely rotating grains. Plotting the vertices curve for this hyperbola ensures that the full range in stable-sink orientation is represented. Several outliers are present outside of the vertices curve in the positive and negative fields. Using the enveloping hyperbola with an opening angle of 53° yields a $W_m = 0.60$ that agrees with the limited rotating and infinitely rotating porphyroclasts. The average orientation (~28°) of shear bands is also shown on the PHD plot.

The RGN demonstrates how the distribution of tailless porphyroclasts in sample G05-01 compares with the predicted transitions to define R_c (Fig. 7A). B^*, as defined by positively inclined porphyroclasts, yields a $W_m = 0.57$ whereas the negatively inclined porphyroclasts define a $W_m = 0.60$. A cluster of positively oriented porphyroclasts plots slightly above the vertices curve on the RGN. We attribute this to either porphyroclasts rotating towards the stable-sink position or as an error of ±3° in defining the foliation for these measurements. Other potential contributors to this error have previously been outlined by Passchier (1987). Porphyroclasts with $B^* > 0.6$ and $\theta < \theta$ at R_c define a lateral cluster close to the vertices curve. Porphyroclasts continue to reach, but remain under, the vertices curve until $B^* < W_m$ at which point porphyroclasts are no longer in a stable-sink position and begin to rotate infinitely (Fig. 7A).

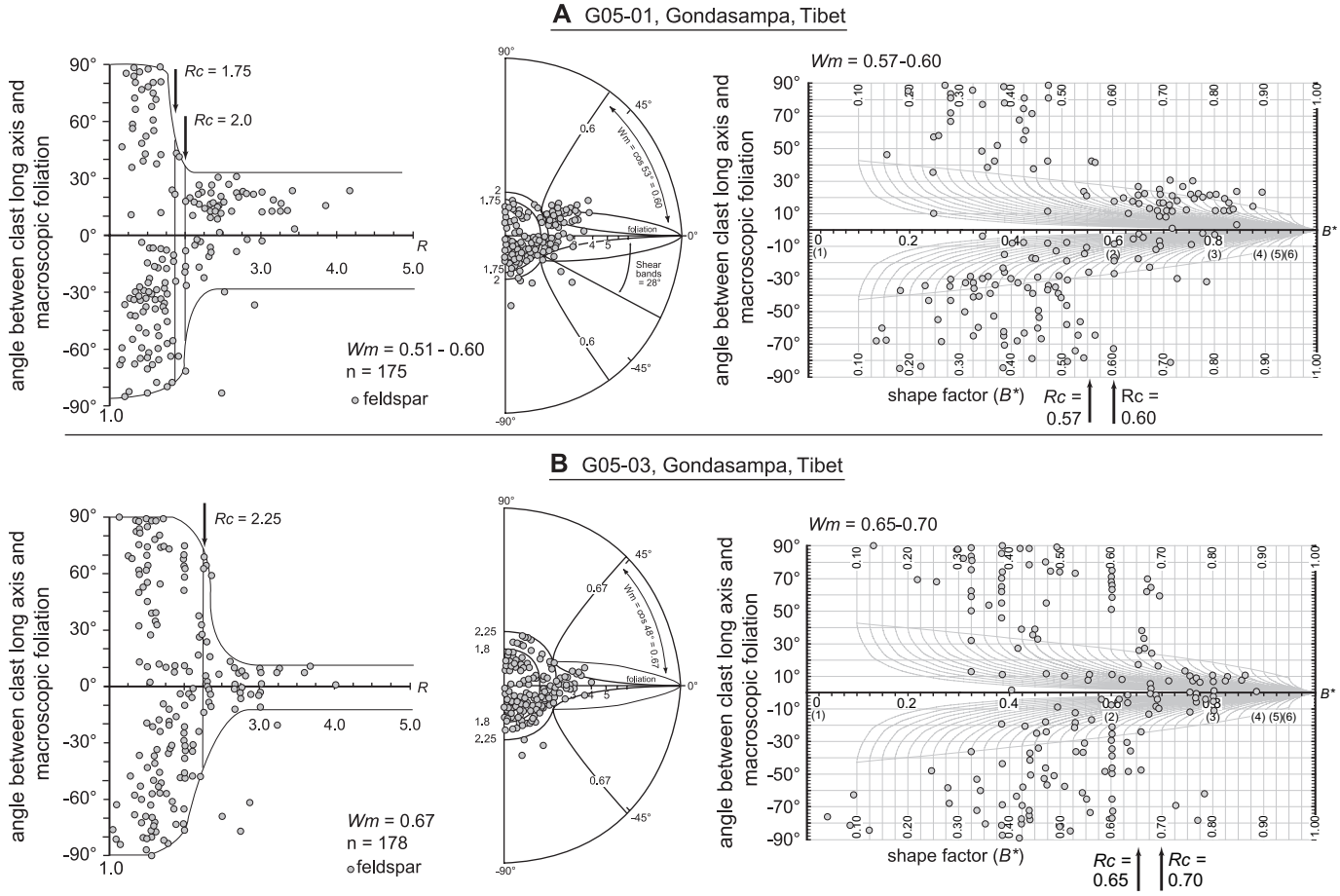

Fig. 7. Samples G05-01 (A; collected at an altitude of 5695 m) and G05-03 (B; collected at an altitude of 5765 m) from the South Tibetan detachment exposed near Gondasampa, Tibet. The Wallis plot (left), PHD plot (center), and RGN (right) are shown for each sample to demonstrate relationships between the three methods. Notice that all porphyroclasts are treated as tailless. See text for details.

Sample G05-03 ($n = 178$) displays a well-defined R_c on the Wallis plot that yields a W_m estimate of 0.67 (Fig. 7B). Rather than relying on three outliers to define R_c and thereby W_m, as with G05-01, we prefer to rely on the majority of tailless porphyroclasts to define R_c. Tailless porphyroclasts are plotted on the HN using the same methods as described in detail for sample G05-01. Two circles define the upper- and lower-limits to the infinitely rotating grains ($R_c = 1.8–2.25$). Two hyperbolas and their vertices curves enclose the remaining porphyroclasts to define a $W_m = 0.67$. When plotted on the RGN, porphyroclasts from sample G05-03 define a range in W_m values between ~0.65 (defined by grains in the negative field) and ~0.70 (defined by grains in the positive field) that agrees with the Wallis plot and the PHD method (Fig. 7B). θ and R values of the majority of tailless porphyroclasts, instead of the three outlying points, are used to define R_c. The compatibility between W_m estimates generated for samples, using tailless porphyroclasts, demonstrate that the RGN unifies the Wallis and PHD methods (Fig. 7).

Two comparisons are made to demonstrate how the RGN limits ambiguity in estimating W_m. The first contrasts the porphyroclast distribution from sample R05-08 on a Wallis plot and the RGN (Fig. 8A). The second plots the porphyroclast distribution defined by Passchier's (1987) data set from the St. Barthelemy Massif using both the Passchier plot and the RGN (Fig. 8B). The sample number in R05-08 is limited ($n = 81$) due to the large porphyroclast size. This gradation in values is more typical of previously published Wallis plots (e.g., Xypolias and Doutsos, 2000; Xypolias and Koukouvelas, 2001; Law et al., 2004; Jessup et al., 2006) than the

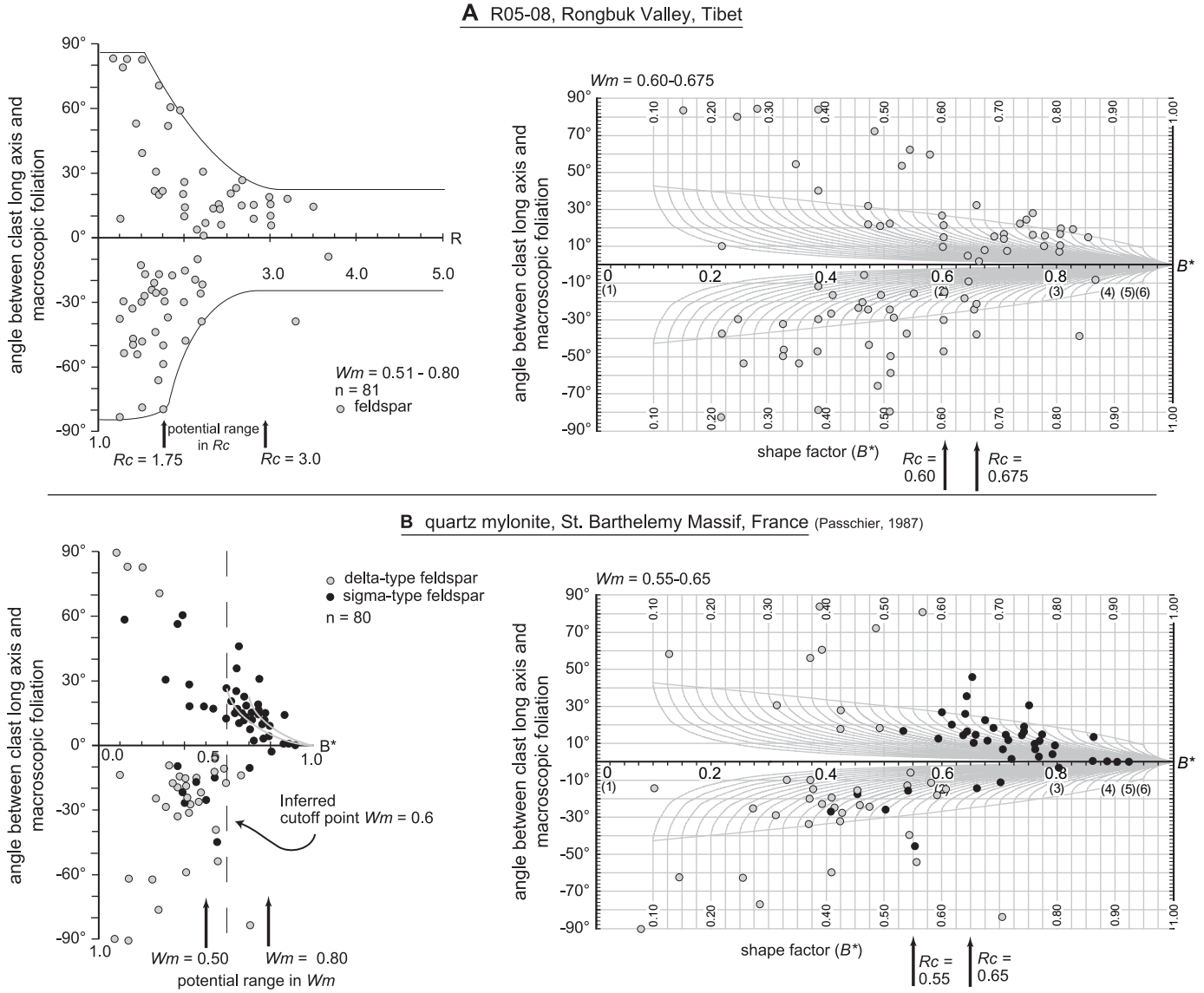

Fig. 8. (A) Porphyroclasts from sample R05-08 from Rongbuk Valley, Tibet (collected several 100 m south of the Northern Transect of Jessup et al. (2006) at an altitude of 4840 m) plotted using both the RGN and the Wallis plot. (B) Porphyroclasts from a quartz mylonite sample from the St. Barthelemy Massif, France from Passchier (1987; his Fig. 10) plotted on the RGN and the original Passchier plot. See text for details on how these comparisons demonstrate that the RGN helps limits ambiguity in estimating W_m.

relatively well-defined R_c values in the Wallis plots for samples G05-01 and 03 (Fig. 7). Without an understanding of which porphyroclasts are predicted to define R_c, the values estimated by different interpretations of this Wallis plot could range from $R = 1.75$ to 3.0, resulting in W_m estimates of 0.51–0.80 (Fig. 8A). When plotted using the RGN, the relative importance of porphyroclasts can be evaluated. For example, at higher B^* values the majority of porphyroclasts fall within the vertices curves in the positive and negative fields. One outlier in the negative field may be significant, but since it is a single analysis we caution against using it to define W_m. Instead, we use the transition defined by porphyroclasts in the positive and negative fields that correspond to a range of $W_m = 0.60–0.675$. This comparison demonstrates that the RGN reduces the potential range in R_c values, as defined by the Wallis plot ($W_m = 0.51–0.80$), to 0.60–0.675 and also helps clarify which porphyroclasts should be used to define R_c.

Using the distribution of porphyroclasts with delta- or sigma-type tails on the original Passchier plot, Passchier (1987) estimated a range of $W_m = 0.50–0.80$ and an inferred cutoff point of $W_m = 0.60$ for a quartz mylonite from the St. Barthelemy Massif, France (Fig. 8B). When plotted on the RGN, these same data define a transition above the vertices curve at $W_m = 0.65$ in the positive field and $W_m = 0.55$ in the negative field. Two outliers that plot above the vertices curves to define higher W_m estimates are excluded in order to maintain consistency with the earlier interpretations and emphasize the use of the majority data to constrain R_c. The RGN also demonstrates that although a single porphyroclast defines a $W_m = 0.48$, it is lower than the majority of grains that define a $W_m = 0.55–0.65$. This comparison highlights how the modified version of the Passchier plot that forms the basis of the RGN, can help limit ambiguity in estimating W_m.

As suggested by results from the four methods applied to the four samples discussed above, Wallis, PHD, Passchier and RGN plots yield consistent W_m estimates. Tailless porphyroclasts can define W_m on the HN, as demonstrated by using two hyperbolas in conjunction with a section of the vertices curves and a circle that envelope the infinitely rotating grains. The same results, however, are more easily plotted and less ambiguously interpreted using the RGN. The range in W_m estimated by the PHD, RGN and Wallis plots from the three natural test samples are within the range of those previously obtained using the Wallis and PHD plots in Rongbuk Valley, Tibet (Law et al., 2004; Jessup et al., 2006).

We limit this approach to the idealized models and a simple comparison between theoretical and natural data using four different plots (Figs. 7 and 8), to clearly present the RGN as an alternative method to estimate W_m. However, many exceptions to these idealized parameters do exist, i.e., plane strain vs. non-plane strain and monoclinic vs. triclinic shear (Giorgis and Tikoff, 2004; Bailey et al., in press). Additionally, the sample must meet the five main requirements defined by Passchier (1987): (1) reasonably homogeneous deformation on the scale of the sample, (2) significant difference in grain size between the rigid porphyroclasts and the matrix, (3) high finite strain to rotate objects towards stable-sink positions, (4) porphyroclast shape that is close to orthorhombic, and (5) significant number of porphyroclasts with a range in aspect ratios and orientations. We also caution against over interpretation of W_m estimates. Future investigations may find that the RGN provides additional information necessary to tackle more complex problems such as triclinic shear and the distribution of tailed vs. tailless porphyroclasts.

5. Conclusions

By building on the original work of Passchier (1987), we have created the RGN as an alternative method to estimate W_m and thereby unify rigid porphyroclast vorticity techniques that were previously proposed by Passchier (1987; Passchier plot), Simpson and De Paor (1993, 1997; PHD plot) and Wallis (1995; Wallis plot). The RGN provides a series of modified semi-hyperbolas that define the predicted orientation of rotating porphyroclasts against which natural, more complex data can be compared: a major advantage over existing methods. Because the same fundamental equations are used to construct the hyperbolas of the RGN and HN, they provide the same theoretical relationships against which natural data can be compared. To test this hypothesis, we used tailless porphyroclasts to constrain the transition between the stable-sink position and infinitely rotating porphyroclasts that define R_c and associated W_m. A comparison of W_m results from four test samples, using the Passchier, Wallis, PHD and RGN plots, demonstrates that the four methods yield internally consistent W_m estimates. By unifying these methods using tailless porphyroclasts, we confirm that tailless porphyroclasts yield W_m estimates that are at least as rigorous as those obtained using methods that rely on tailed porphyroclast, i.e., the PHD method and Passchier plot. Through comparisons between how the distribution of less-than-ideal data from sample R05-03 defines W_m using the Wallis plot vs. the RGN and between the Passchier plot and the RGN, we demonstrate that contrasting porphyroclast distributions with the orientations predicted by the RGN can help limit ambiguity in estimating W_m.

Another benefit of the RGN is that data from porphyroclasts can be entered into an Excel© worksheet and plotted directly on the RGN which can be imported as a background to an Excel© chart. This enables immediate feedback on the significance of each porphyroclast. The W_m curves on the RGN offer an easier means to define R_c within a sample and should help refine and standardize the results of future investigations. Because of its ease of use, ability to enhance and justify the choice of R_c, and potential to calibrate the presentation of various investigations, we offer the RGN as an alternative approach to estimating W_m in high strain zones.

Acknowledgements

We thank Dennis Newell and John Cottle for their motivated efforts in the field and unnerving capacity to present the counter-hypothesis as well as Sonam Wangdu who brought

us to his home, Gondasampa, where we collected the samples that formed the basis of this investigation. Also, we greatly appreciated insightful discussions with Jeff Lee, Benjamin Schwartz and Ryan Thigpen that helped clarify many sections of the manuscript. Many thanks to C. Bailey, D. De Paor, S. Wallis and P. Xypolias whose reviews greatly strengthened this manuscript. The expedition to Gondasampa and Rongbuk Valley (2005) was funded by a 2010 Fellowship from the College of Science, Virginia Tech and a Geological Society of America research grant to MJJ as well as a New Zealand TEC Bright Future Top Achiever Doctoral Scholarship to John Cottle.

Appendix A. Supplementary information

Supplementary data associated with this article can be found, in the online version, at doi:10.1016/j.jsg.2006.11.003.

References

Bailey, C.M., Polvi, L.E., Forte, A.M. Pure shear-dominated high-strain zones in basement terranes. In: Hatcher Jr., R.D., Carlson, M.P., McBride J.H., Catalán, J.R.M. (Eds.), Four-Dimensional Framework of Continental Crust, Geological Society of America Memoir, in press.

Bailey, C.M., Eyster, E.L., 2003. General shear deformation in the Pinaleno Mountains metamorphic core complex, Arizona. Journal of Structural Geology 25, 1883–1893.

Bretherton, F.P., 1962. The motion of rigid particles in shear flow at low Reynolds number. Journal of Fluid Mechanics 14, 284–301.

De Paor, D.G., 1983. R_f/ϕ_f strain analysis using an orientation net. Journal of Structural Geology 10, 323–333.

Ghosh, S.K., Ramberg, H., 1976. Reorientation of inclusions by combination of pure and simple shear. Tectonophysics 34, 1–70.

Giorgis, S., Tikoff, B., 2004. Constraints on kinematics and strain from feldspar porphyroclast populations. In: Alsop, G.I., Holdsworth, R.E., McCaffrey, K.J.W., Hand, M. (Eds.), Flow Processes in Faults and Shear Zones. Geological Society, London, Special Publications, vol. 224, pp. 265–285.

Hirth, G., Tullis, J., 1992. Dislocation creep regimes in quartz aggregates. Journal of Structural Geology 14, 145–160.

Holcombe, R.J., Little, T.A., 2001. A sensitive vorticity gauge using rotated porphyroblasts and its application to rocks adjacent to the Alpine Fault, New Zealand. Journal of Structural Geology 23, 979–990.

Jeffery, G.B., 1922. The motion of ellipsoidal particles immersed in a viscous fluid. Proceedings of the Royal Society of London A102, 161–179.

Jessup, M.J., Law, R.D., Searle, M.P., Hubbard, M.S., 2006. Structural evolution and vorticity of flow during extrusion and exhumation of the Greater Himalayan Slab, Mount Everest Massif, Tibet/Nepal: implications for orogen-scale flow partitioning. In: Law, R.D., Searle, M.P., Godin, L. (Eds.), Channel Flow, Extrusion, and Exhumation in Continental Collision Zones. Geological Society, London, Special Publications, vol. 268, pp. 379–414.

Klepeis, K.A., Daczko, N.R., Clarke, G.L., 1999. Kinematic vorticity and tectonic significance of superposed mylonites in a major lower crustal shear zone, northern Fiordland, New Zealand. Journal of Structural Geology 21, 1385–1406.

Law, R.D., Searle, M.P., Simpson, R.L., 2004. Strain, deformation temperatures and vorticity of flow at the top of the Greater Himalayan Slab, Everest Massif, Tibet. Journal of the Geological Society, London 161, 305–320.

Murphy, M.A., Harrison, T.M., 1999. Relationship between leucogranites and the Qomolangma detachment in the Rongbuk Valley, south Tibet. Geology 27, 831–834.

Passchier, C.W., 1987. Stable positions of rigid objects in non-coaxial flow – a study in vorticity analysis. Journal of Structural Geology 9, 679–690.

Simpson, C., De Paor, D.G., 1993. Strain and kinematic analysis in general shear zones. Journal of Structural Geology 15, 1–20.

Simpson, C., De Paor, D.G., 1997. Practical analysis of general shear zones using porphyroclast hyperbolic distribution method: an example from the Scandinavian Caledonides. In: Sengupta, S. (Ed.), Evolution of Geological Structures in Micro- to Macro-scales. Chapman and Hall, London, pp. 169–184.

Stipp, M., Stunitz, H., Heilbronner, R., Schmid, S., 2002. Dynamic recrystallization of quartz: correlation between natural and experimental conditions. In: De Meer, S., Drury, M.R., De Bresser, J.H.P., Pennock, G.M. (Eds.), Deformation Mechanisms, Rheology and Tectonics: Current Status and Future Perspectives. Geological Society, London, Special Publications, vol. 200, pp. 171–190.

Vissers, R.L.M., 1989. Asymmetric quartz *c*-axis fabrics and flow vorticity: a study using rotated garnets. Journal of Structural Geology 11, 231–244.

Wallis, S.R., 1992. Vorticity analysis in a metachert from the Sanbagawa Belt, SW Japan. Journal of Structural Geology 14, 271–280.

Wallis, S.R., 1995. Vorticity analysis and recognition of ductile extension in the Sanbagawa belt, SW Japan. Journal of Structural Geology 17, 1077–1093.

Wallis, S.R., Platt, J.P., Knott, S.D., 1993. Recognition of syn-convergence extension in accretionary wedges with examples from the Calabrian Arc and the Eastern Alps. American Journal of Science 293, 463–495.

Xypolias, P., Doutsos, T., 2000. Kinematics of rock flow in a crustal scale shear zone: implications for the orogenic evolution of the southwestern Hellenides. Geological Magazine 137, 81–96.

Xypolias, P., Koukouvelas, I.K., 2001. Kinematic vorticity and strain patterns associated with ductile extrusion in the Chelmos shear zone (External Hellenides, Greece). Tectonophysics 338, 59–77.

Xypolias, P., Kokkalas, S., 2006. Heterogeneous ductile deformation along a mid-crustal extruding shear zone: an example from the External Hellenides (Greece). In: Law, R.D., Searle, M.P., Godin, L. (Eds.), Channel flow, Extrusion, and Exhumation in Continental Collision Zones. Geological Society, London, Special Publications, vol. 268, pp. 497–516.